Progress In Electromagnetics Research M, Vol. 114, 1–12, 2022

A Miniaturized Reconfigurable Quad-Band Bandpass Filter with W-Shaped SIRs

Ren Wang[1], Tao Tang[2, *], Melad M. Olaimat[3], Yuanzhi Liu[4], Omar M. Ramahi[5], and Zhu Jin[2]

Abstract—A novel quad-band bandpass filter (BPF) consisting of two deformed W-shaped microstrip Stepped-Impedance Resonators (SIRs) with different dimensions is proposed. The W-shaped SIRs are miniaturized from E-shaped SIRs, and each one of the SIRs generates two passbands and thus four passbands centered at 3.18 GHz, 4.51 GHz, 5.46 GHz, and 8.43 GHz with fractional bandwidth of 6.7%, 9.1%, 8.4%, and 8.2% were obtained. Compared with the basic SIR structures and E-shaped structures, the effective area of the miniaturized SIR is reduced by more than 60% and 20%, respectively. The operating frequency bands can be determined by switching the diodes that are connected to the cross coupling lines of the two SIRs. The improved design can be used for 5G and other applications.

1. INTRODUCTION

Multi-band bandpass filters (BPFs), which are key components of wireless systems, have become increasingly important with the rapid growth of multi-service wireless communication networks [1]. Many different BPFs with different operation bands have been proposed in recent years to achieve this goal [2–6]. Various techniques, such as loading distributed capacitors in the inner area of conventional dual-mode loop resonators [7], employing meander-loop resonators [8, 9], open loop resonators, and hybrid loading different resonators, can be used to produce dual-band operations.

Because of their spurious frequency response to create a higher passband, the stepped impedance resonators (SIRs) have been employed to create dual-band BPFs [10–13]. As a result, generating another passband utilizing single-band SIR BPFs is feasible.

Frequency reconfigurable filters allow for circuit simplifications and the implementation of advanced capabilities in complicated subsystems, which is crucial for future communications system applications [14]. As a result, in recent years, some reconfigurable filters have been proposed in which different resonant responses are achieved by adjusting the dimensions of the resonant elements [15, 16]. However, increasing the length of the resonator as a reconfiguration option has significant challenges that are difficult to overcome in practice.

We previously presented a quad-band BPF with two E-shaped SIRs and two cross-coupling structures between the input and output feed lines [17]. Each one of the E-shaped SIRs corresponds to the first four resonant frequencies, and two passbands can be easily created after combining with the cross-coupling lines that generate three transmission zeros. Additionally, one of the E-shaped SIRs can be selected to work and control the passbands of the proposed BPF by connecting or disconnecting the

Received 19 June 2022, Accepted 3 October 2022, Scheduled 8 October 2022

* Corresponding author: Tao Tang (tangt@cuit.edu.cn).

[1] School of Electronic Science and Engineering, University of Electronic Science and Technology of China, Chengdu, Sichuan 611731, China. [2] College of Electronic Engineering, Chengdu University of Information Technology, Chengdu, Sichuan 610225, China. [3] Department of Renewable Energy, University of AL Albayt, Al-Mafraq 25113, Jordan. [4] Edward S. Rogers Sr. Department of Electrical and Computer Engineering, University of Toronto, Toronto, ON M5S 3G4, Canada. [5] Department of Electrical and Computer Engineering, University of Waterloo, Waterloo N2L 3G1, Canada.

cross-coupling lines corresponding to the two SIRs with the middle common feed lines, resulting in a choice between two sets of dual operating bands.

In this paper, we present a downsizing method for BPF to reduce its size without compromising its performance. The miniaturized design incorporates new SIRs that are deformed W-shaped. Compared to the original design, this design is approximately 20% smaller, while the performance is maintained. Furthermore, the loading of diodes at the slots between the cross-coupling lines and the feed line is proposed to enable switching between different operating modes. Controlling the functioning state of the diode allows two sets of operating passbands to be swapped.

2. BASIC CONFIGURATION OF SIRS

2.1. Fundamental Theories

The structure of the widely used half-wavelength SIR is illustrated in Fig. 1, which can be seen as three two-port networks cascaded together. Suppose that the impedance ratio of Z_1 and Z_2 is K ($K = Z_2/Z_1 > 1$), then the admittance at the input terminal of the structure is:

$$Y_{in} = jY_2 \cdot \frac{2(K\tan\theta_1 + \tan\theta_2)\cdot(K - \tan\theta_1\cdot\tan\theta_2)}{K(1-\tan^2\theta_1)\cdot(1-\tan^2\theta_2) - 2(1+K^2)\cdot\tan\theta_1\cdot\tan\theta_2}, \tag{1}$$

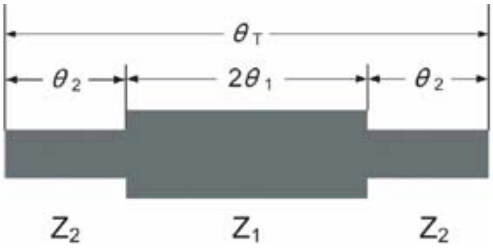

Figure 1. Basic structure of a half-wavelength SIR.

From Eq. (1), the resonance condition ($Y_{in} = 0$) can be obtained when $K = \tan\theta_1 \cdot \tan\theta_2$. Assuming $\theta_1 = \theta_2 = \theta$, then the electrical length of the two shorter SIRs at both end should be $\theta = \arctan\sqrt{K}$, and the electrical length of the middle microstrip line of the SIR is 2θ. With these conditions, Eq. (1) can be rewritten as:

$$Y_{in} = jY_2 \cdot \frac{2(K+1)\cdot(K-\tan^2\theta)\cdot\tan\theta}{K - 2(1+K-K^2)\cdot\tan\theta}, \tag{2}$$

Suppose that the fundamental frequency of an SIR with multiple stages is f_1, and the first three higher resonances are f_2, f_3, and f_4 that correspond to electrical lengths of θ_2, θ_3, and θ_4, respectively. Then the following equations can be obtained from Eq. (2):

$$\begin{aligned} &K\cdot\tan\theta_2 = \infty \\ &\tan^2\theta_3 - K = 0, \\ &\tan\theta_4 = 0 \end{aligned} \tag{3}$$

From Eq. (3), we can obtain the corresponding electrical lengths as:

$$\begin{aligned} &\theta_2 = \pi/2 \\ &\theta_3 = \tan^{-1}(-\sqrt{K}) = \pi - \theta \\ &\theta_4 = \pi \end{aligned} \tag{4}$$

From Eq. (4), the relationship between the operating frequencies of the SIR can be determined by their corresponding electrical lengths as follows:

$$\begin{aligned} \frac{f_2}{f_1} &= \frac{\theta_2}{\theta_1} = \frac{\pi}{2\arctan\sqrt{K}} \\ \frac{f_3}{f_1} &= \frac{\theta_3}{\theta_1} = 2\left(\frac{f_2}{f_1}\right) - 1 \\ \frac{f_4}{f_1} &= \frac{\theta_4}{\theta_1} = 2\left(\frac{f_2}{f_1}\right) \end{aligned} \quad . \tag{5}$$

Obviously, the resonant frequencies of the SIR depend on the impedance ratio (K). The impedance ratio can be controlled by adjusting the length of either center and/or terminal microstrip lines. Consequently, all responses of the design are predictable and can be controlled.

Figure 2 shows the configuration of the basic SIR with a cross-coupling line and the simulated S-parameters. Setting $K = 2$ and $f_1 = 3.0\,\text{GHz}$ in equation Eq. (5), the frequency ratio $f_2/f_1 \approx 1.4$, $f_3/f_1 \approx 1.8$, and $f_4/f_1 \approx 2.8$, consequently, $f_2 \approx 4.2\,\text{GHz}$, $f_3 \approx 5.4\,\text{GHz}$, and $f_4 \approx 8.4\,\text{GHz}$. It can be noted that the simulation results are in good agreement with the predicted ones.

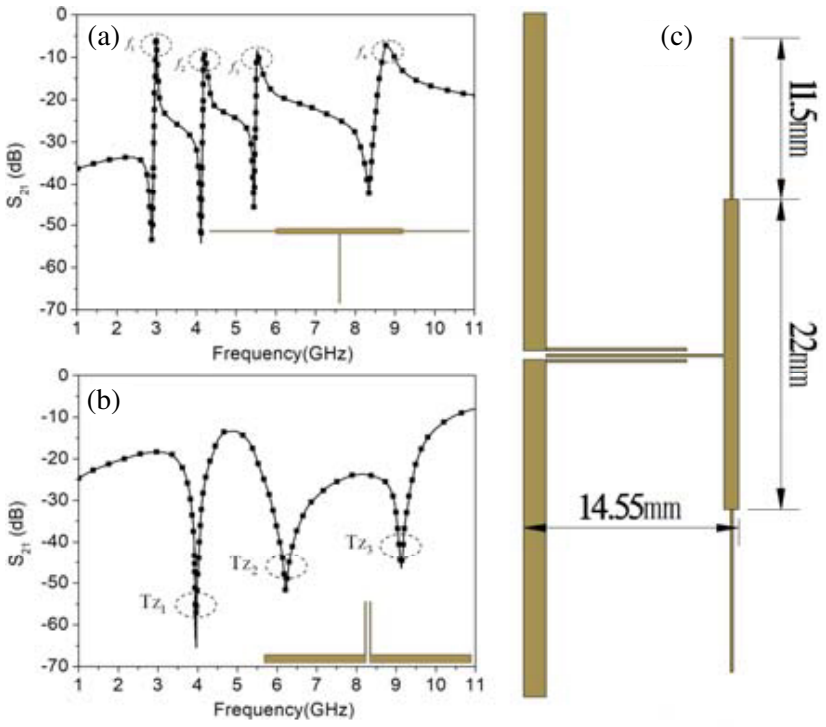

Figure 2. (a) The first four resonances of the SIR. (b) Transmission zeros of the cross-coupling line. (c) Configuration of the basic SIR with a cross-coupling line.

Due to the first four resonances of the SIR and the multiple transmission zeros created by the cross-coupled line, connecting a cross-coupled line to the input and output feed lines of the SIR structure can result in multiple passbands. The transmission zeros of the cross-coupling line are given in Fig. 2(b). Therefore, by adjusting the length of the SIR and cross-coupling line, the first two resonant modes and the first transmission zero (Tz_1) can be formed into two passbands. The second and third transmission zeros (Tz_2 and Tz_3) can provide a better band-stop effect at the high frequency band.

2.2. Dual Deformed W-Shaped SIRs

According to the fundamental theories, a quad-band BPF based on the dual SIRs with cross-coupling lines has been proposed. In order to reduce the effective area of the basic SIR, the terminal lines of the SIR were bent to form deformed W-shape. Fig. 3 displays the structure of the proposed quad-band BPF of dual deformed W-shaped SIRs, which consists of a ground plane, two deformed W-shaped SIRs with different dimensions, and two sets of cross-coupling lines corresponding to each deformed W-shaped SIR. The two sets of cross-coupling lines are connected in the middle to the common feed line.

The large deformed W-shaped SIR in Fig. 3(a) supports the two lower passbands of the quad-band BPF, whereas the small deformed W-shaped SIR in Fig. 3(b) supports the two higher passbands of the quad-band BPF. Fig. 3(c) illustrates the overall configuration of the quad-band BPF and the partial enlargement of the slots created on the cross-coupling lines. Fig. 3(d) depicts a fabricated prototype of the proposed design. The design was fabricated on a Rogers substrate (RO 4350C) with a thickness of 0.508 mm and relative permittivity of 3.66. The dimensions are provided in Table 1.

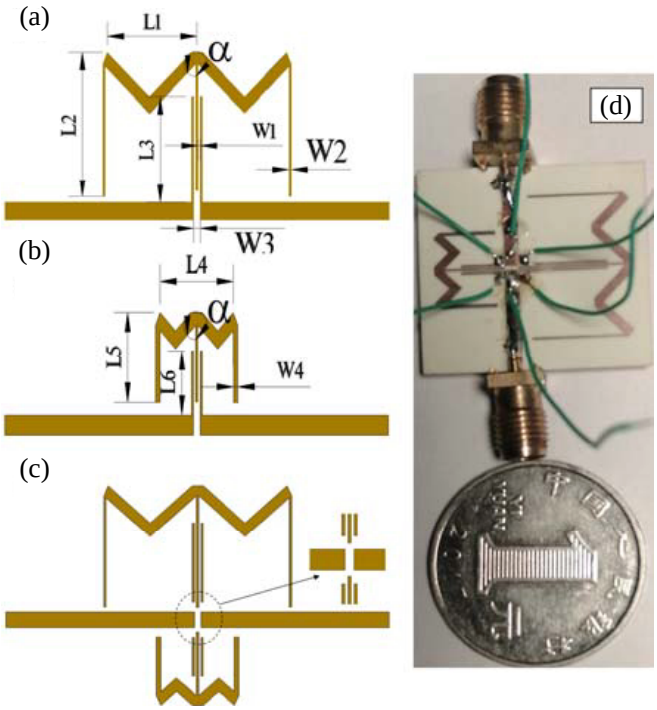

Figure 3. Configuration of the dual deformed W-shaped SIRs quad-band BPF. (a) The large deformed W-shaped SIR. (b) The small deformed W-shaped SIR. (c) Over all structure. (d) The prototype.

Table 1. Dimensions of the deformed W-shaped SIRs quad-band BPF (mm and degree).

Parameters	L_1	L_2	L_3	L_4	L_5	L_6	W_1	W_2	W_3	W_4	α
Values	8.15	12.5	10.2	6.69	7.5	5.1	0.2	0.2	0.8	0.5	45

Figure 4(a) presents the simulation results of this design when all four side lines of the cross-coupling lines are connected to the feed line. In this case, both the larger (denoted as SIR1) and smaller (denoted as SIR2) deformed W-shaped SIRs are working simultaneously to provide four passbands. The first, second, third, and fourth passbands are 3.07–3.29 GHz, 4.29–4.73 GHz, 5.29–5.71 GHz, and 8.07–8.78 GHz, which are centered at 3.18 GHz, 4.51 GHz, 5.46 GHz, and 8.43 GHz, respectively. The fractional bandwidth of each passband in order are 6.7%, 9.1%, 8.4%, and 8.2%.

Figures 4(b) and (c) illustrate the simulation results of SIR1 and SIR2 when they work separately.

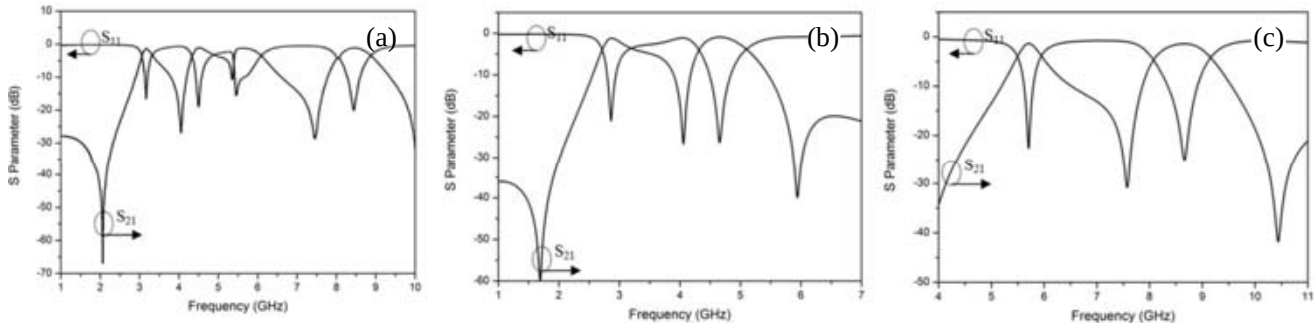

Figure 4. Simulation results. (a) Both cross-coupling lines of SIR1 and SIR2 are connected to the feed line. (b) Only cross-coupling lines of SIR1 is connected to the feed line. (c) Only cross-coupling lines of SIR2 is connected to the feed line.

When the two cross-coupling lines of SIR1 are connected to the feed line and those of SIR2 disconnected, the BPF has only the first and second passbands. On the other hand, the BPF has the third and fourth passbands when cross-coupling lines of SIR2 are connected to the feed line and those of SIR1 disconnected. Such a special feature allows the design of a frequency reconfigurable BPF.

3. MINIATURIZATION AND DESIGN PROCESS

3.1. Miniaturization

By comparing Fig. 2(c) and Fig. 3(a), it can be observed that the effective area will be reduced by 62% (the effective width of basic SIR will be lowered from 45 mm to 16.3 mm) if the length of each portion of SIR is kept constant. By bending the resonant arms at both ends to form a deformed W-shape structure, the effective area is lowered from 655 mm^2 to 249 mm^2.

The proposed deformed W-shaped SIRs BPF is a miniaturization design based on the E-shaped SIRs [17]. We will present the design process in this section. By bending the two terminal lines of the SIR to form E-shaped SIRs, the effective area has been reduced by 52% (the effective width of the basic SIR has been lowered from 45 mm to 21.6 mm, and the effective area was lowered from 655 mm^2 to 314 mm^2).

The E-shaped SIR can be bent into a W-shaped SIR by bending it further. As illustrated in Fig. 5(a), the length of the middle lateral component of the E-shaped SIR1 is kept constant and bent

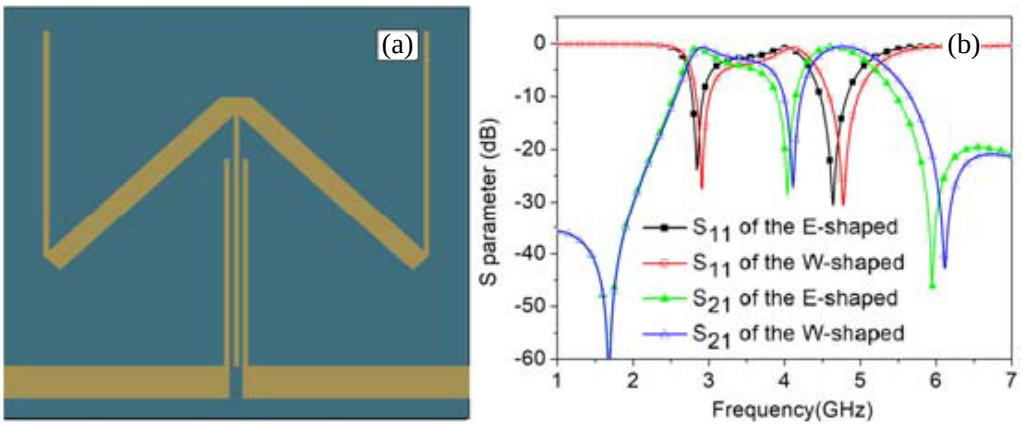

Figure 5. W-shaped SIR. (a) Configuration. (b) *S*-parameters of E-shaped SIR1 and the W-shaped SIR1.

in the direction of the feed line. After bending, the resonant arms on both sides create a W-shaped structure. With this adjustment, the SIR1's effective area can be lowered by 53% (from 655 mm^2 to 305 mm^2) compared to the basic SIR structure and by 2.9% (from 314 mm^2 to 305 mm^2) compared to the E-shaped structure. The passbands, however, are all pushed toward higher frequencies, as illustrated in Fig. 5(b). Fortunately, these changes can be overcome by altering the length of each portion of the W-shaped SIR.

Furthermore, as depicted in Fig. 6(a), this W-shaped structure can be further twisted to form a deformed W-shaped structure with resonant arms on both sides. The degree of bending can be changed to increase or decrease the effective area of the SIR by adjusting the value of α. The high and low passbands of the deformed W-shaped SIR will increase as the bending angle α lowers, as shown in Fig. 6(b). The narrower the bend angle is, the bigger the effective area reduction can be deduced from Fig. 6(a).

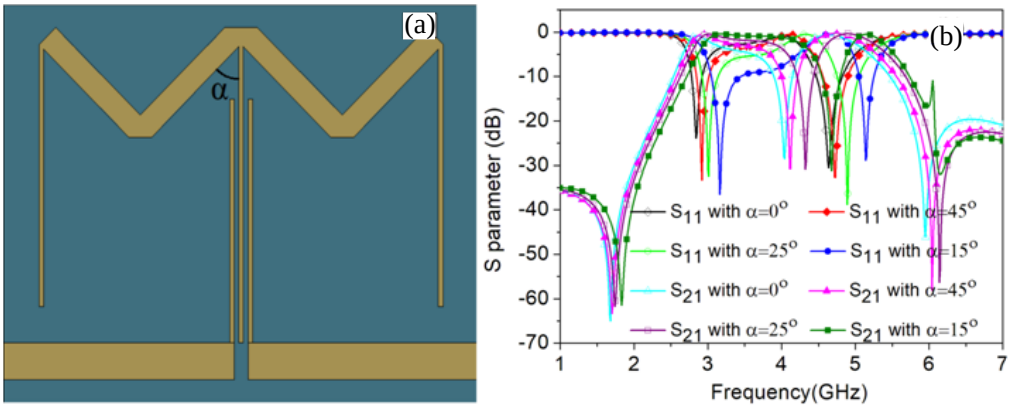

Figure 6. Deformed W-shape SIR and its S-parameters. (a) Configuration. (b) S-parameters with different bending angles.

As demonstrated in Fig. 6(b), when the middle resonant arm of this E-shaped SIR is bent at an angle of $\alpha = 45°$, there is little influence on the two passbands. However, the effective area of the deformed W-shaped SIR structure is reduced by 62% compared with the basic SIR structure. Compared with the E-shaped structure, the effective area of deformed W-shaped structure is reduced by 21% (from 314 mm^2 to 249 mm^2).

Because additional microstrip lines are required for connection at the turning point of the middle bending arm, and the resonant arms on both sides are cut into oblique triangles due to the connection part, the equivalent θ_1 increases, and θ_2 decreases in this deformed W-shaped structure, as shown in Fig. 1. The corresponding high-order resonance frequencies will then increase according to Eq. (5).

Figure 7 compares the transmission characteristics between the deformed W-shaped SIR and E-shaped SIR when $\alpha = 45°$. This figure clearly shows that all resonances of the deformed W-shaped SIR have been shifted towards higher frequencies. According to the fundamental theories, the passband frequency point constituted by the deformed W-shaped SIR and the cross-coupling lines will increase, which verifies our speculation about the shift of this passband of the dual-passband filter to a higher frequency band.

3.2. Design Process

Based on the previously described theories, the design process can be broken down into four steps: To begin, two filters of various dimensions are built separately, and each deformed W-shaped SIR and its cross-coupling lines constitute a dual band BPF, as depicted in Fig. 8(a). To achieve the port isolation criteria, two SIRs are mounted on the same substrate with a specific distance between the feed lines, as shown in Fig. 8(b). The cross-coupling feed lines that connect the two SIRs are then configured to

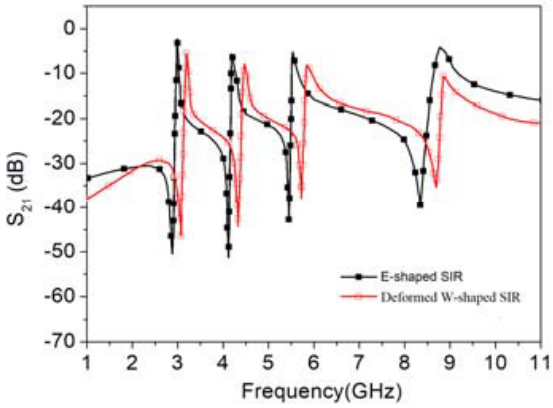

Figure 7. The first four resonant modes of the deformed W-shaped SIR with $\alpha = 45°$ and the E-shaped SIR.

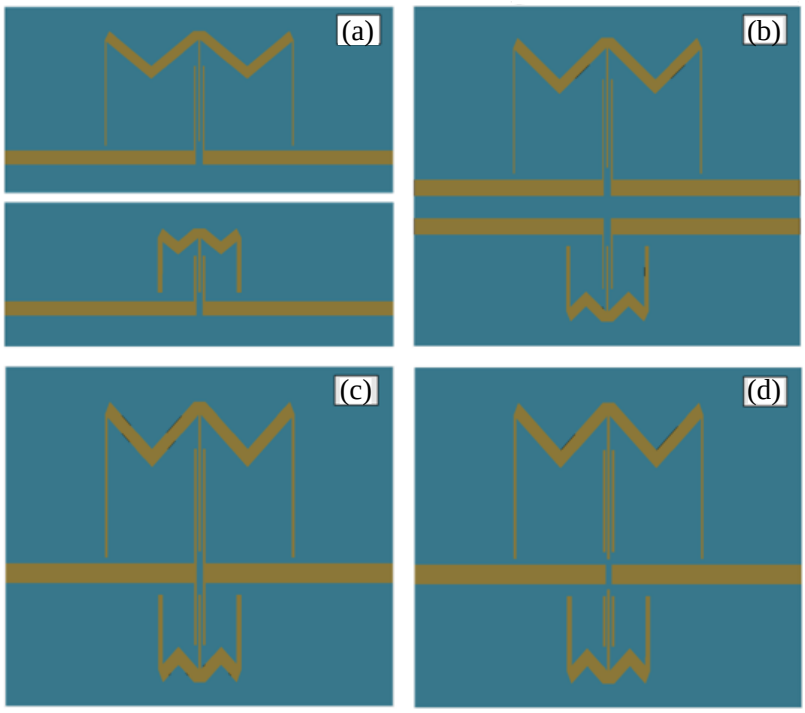

Figure 8. Design process. (a) Two independent deformed W-shaped SIR filters. (b) Share the same substrate. (c) Share the same feed line. (d) Break slots created on the cross-coupling lines.

share a single feed line as displayed in Fig. 8(c). Finally, the cross-coupling lines are disconnected to install the switches as illustrated in Fig. 8(d).

As depicted in Fig. 9(a), when SIR1 and SIR2 are integrated on the same substrate, the isolation of the two input ports increases with the distance between their feed lines. For instance, it is greater than 20 dBc in all desired frequency bands when the distance is larger than 2 mm.

Comparing Figs. 8(b) and (c), we notice that the effective area of this quad-band BPF can be reduced by at least 14% by sharing the same feed line and considering that the port isolation is greater than 20 dBc. Figs. 9(b) and (c) show how the other disconnected SIR affects the performance of the connected SIR by comparing the simulated S-parameters of the design shown in Fig. 8(d) under different operation statuses with those of the design shown in Figs. 4(b) and (c).

From Figs. 9(b) and (c), we can notice that SIR2 has some impact on the resonant frequencies

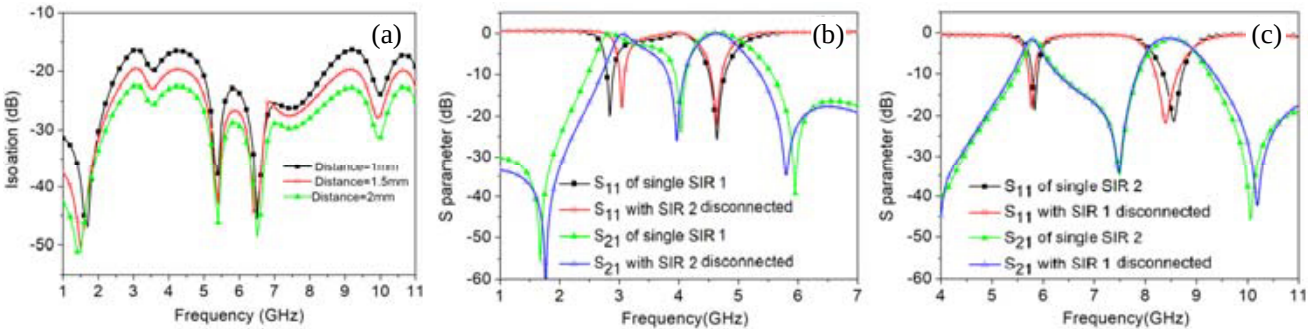

Figure 9. The isolation between the two input ports of SIR1 and SIR2 of Fig. 8(b) and the interaction of two SIRs of Fig. 8(c). (a) Isolation. (b) S-parameters of SIR1 working alone. (c) S-parameters of SIR2 working alone.

of SIR1 even if SIR2 is disconnected. The center of the low-passband of SIR1 shifts slightly towards the higher frequencies while the center of the high-passband remains basically unchanged. Besides, the bandwidth of both passbands is slightly reduced. On the contrary, when SIR1 is disconnected, both passbands of SIR2 shift slightly to lower frequencies, while the bandwidth at two frequencies remains basically unchanged.

4. SWITCHING MECHANISM

Disconnecting and reconnecting the slots on the cross-coupling lines to switch between two sets of passbands cannot meet the requirement of rapid switching in practice. To provide the function of rapid switching, diodes are used to connect the slots. Fig. 10(e) depicts the appropriate positions of the diodes in our design. When the diode is in the on-state, it is equivalent to $0.5\,\Omega$ resistance, and when it is in the off-state, it is equivalent to 0.25 pF capacitance. The influence of the diode in the cross-coupling lines on the S-parameters of each independent SIR in Fig. 8(a) is shown in Figs. 10(a) and (b). From Figs. 10(a) and (b), the use of diodes as switches has negligible effect on the S-parameters of the BPF. Therefore, it is feasible to use diodes to integrate or separate the two SIRs.

For the final minimized design, that is Fig. 8(d), when a high voltage is provided to the middle common feed line in the connection mode shown in Fig. 10(e), the top two diodes (denoted as No. 1) turn on, while the bottom two diodes (denoted as No. 2) remain off. In this condition, the cross-coupling lines corresponding to SIR1 are in the connected state, while the cross-coupling lines corresponding to SIR2 are in the disconnected state. As a result, the SIR1 on the top side will be activated while the SIR2 on the opposite side will not be, resulting in two lower frequency passbands in the design. The S-parameter of the structure in this situation is illustrated in Fig. 10(c). If a low voltage is provided to the common feed line, the No. 1 diodes will be turned off, while the No. 2 diodes will be turned on. Reversing the applied voltage leads to disconnecting SIR1 and connecting the SIR2, and thus the SIR1 will not be working, and the SIR2 will be working, resulting in two higher frequency bands. Under this condition, the S-parameter of the structure is revealed in Fig. 10(d).

If No. 1 and No. 2 diodes are powered separately, the two sets of diodes can be in the on-state at the same time, thus realizing the quad-band BPF with SIR1 and SIR2 working simultaneously. A comparison of the S-parameters of this quad-band BPF with all diodes in on state and the S-parameters of Fig. 4(a) with all slots connected on the cross-coupling lines is shown in Fig. 11. From Figs. 10(c) and (d), it can be found that the mode of switching with diodes has small effect on the interested frequency band of SIR1, but the center frequency point of the higher passband of SIR2 will be shifted by 180 MHz in the direction of high frequency. As can be seen from Fig. 11, introducing diodes keeps all passband widths of the filter almost constant with slight shift in the center frequency, especially for the fourth passband.

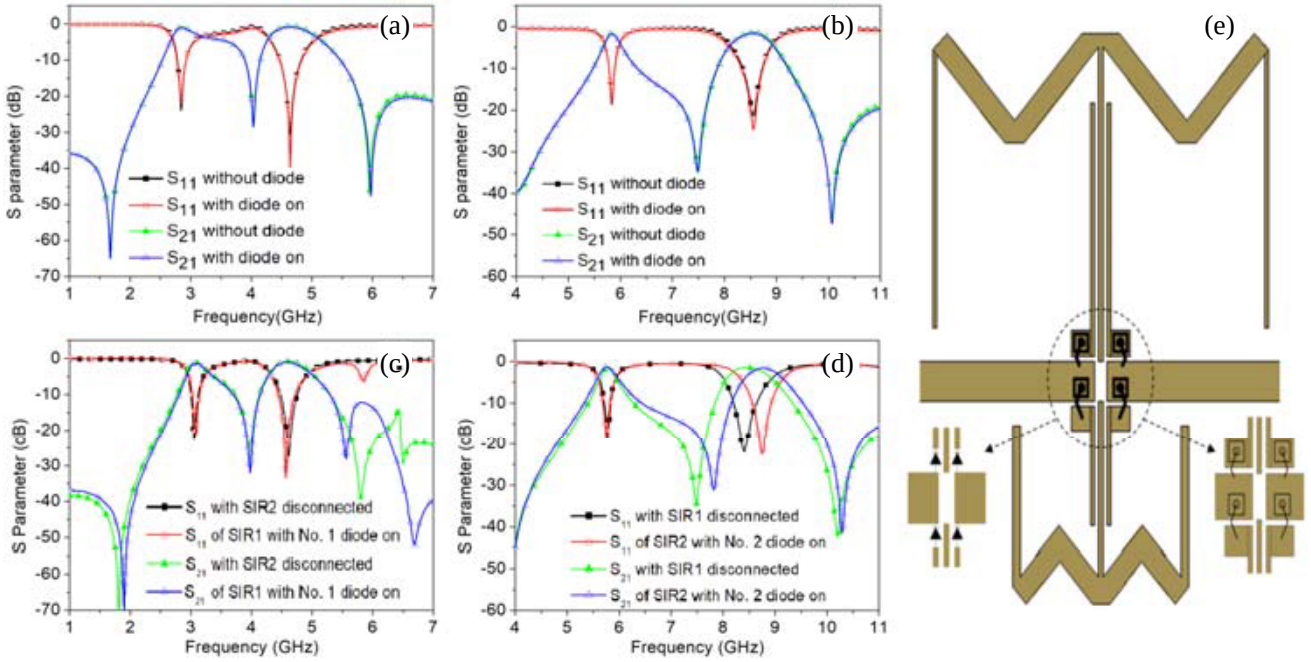

Figure 10. Impacts of diodes and the illustration of the connection position of the diodes. (a) S-parameters of separately SIR1 with and without diode on corresponding cross-coupling lines. (b) S-parameters of separately SIR2 with and without diode on corresponding cross-coupling lines. (c) S-parameters of SIR1 with and without diode on corresponding cross-coupling lines of the final design. (d) S-parameters of SIR2 with and without diode on corresponding cross-coupling lines of the final design. (e) The connection position of the diodes.

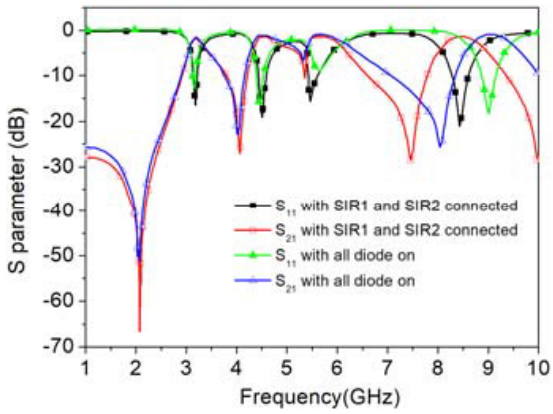

Figure 11. Comparison between S-parameters of the filter with all diodes in on state and the S-parameters of the filter by connect all the slots on the cross-coupling lines.

5. MEASUREMENT RESULTS

A miniaturized quad-band BPF consisting of two deformed W-shaped SIRs with a bending angle of 45° was fabricated, which is shown in Fig. 3(d). The diodes are connected on its appropriate positions through golden wires.

The transmission characteristic of the dual deformed W-shaped SIR BPF shown in Fig. 8(d) was measured with SIR1 and SIR2 connected simultaneously, and the results are shown in Fig. 12(a).

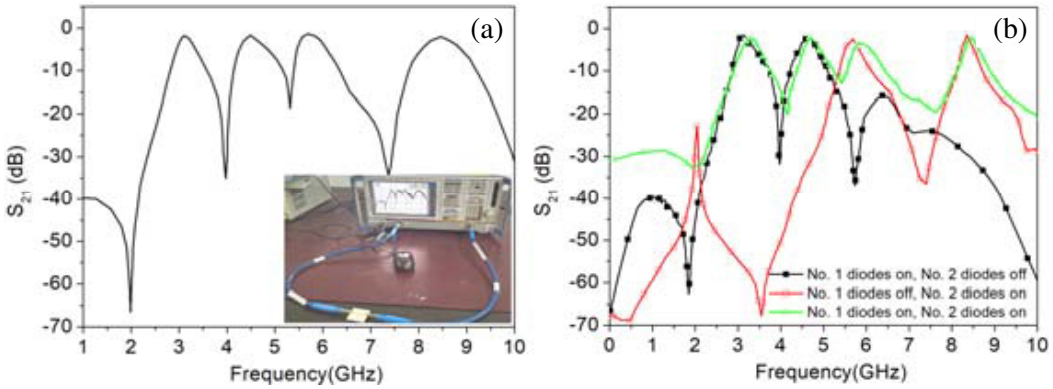

Figure 12. The measured transmission characteristics of the dual deformed W-shaped SIRs BPF. (a) Measured transmission characteristics. (b) Measured transmission characteristics with different working models.

Table 2. Simulation and measurement passbands with different working models (GHz).

Working models	First PB	Second PB	Third PB	Fourth PB
No. 1 diodes on, No. 2 diodes off	sim. 2.95	sim. 4.53	/	/
	mea. 3.06	mea. 4.46	/	/
No. 1 diodes off, No. 2 diodes on	/	/	sim. 5.53	sim. 8.41
	/	/	mea. 5.47	mea. 8.53
No. 1 diodes on, No. 2 diodes on	sim. 3.18	sim. 4.51	sim. 5.46	sim. 8.43
	mea. 3.09	mea. 4.42	mea. 5.52	mea. 8.65

The measured and simulated results are in good agreement. The deformed W-shaped SIRs BPF was measured with diodes utilized as switches. The measurement results are presented in Fig. 12(b), and the comparison results are summarized in Table 2.

Table 3. Comparison among other reported filters.

Ref.	Area (mm^2)	Frequency band (GHz)	Reconfigurable
[3]	/	1.3–1.5, 2.36–2.6, 3–3.54	yes
[4]	$> 445.2/ > 816.96$	1.85–3.03/1.61–1.99, 2.26–2.64	no
[5]	$0.15\lambda_g * 0.15\lambda_g$	2.55, 3.91 with band width of 13%, 5.4%	no
[6]	$0.079\lambda_g * 0.193\lambda_g$	0.9, 1.85 with band width of 16.3%, 10.7%	no
[10]	/	1.576–1.628, 1.558–1.618, 1.550–1.611	yes
[11]	> 7091.92	1.57 with 9.9% band width, 2.38 with 6.5% band width	no
[12]	$0.65\lambda_g * 0.38\lambda_g$ with Roger 5880	1.4, 2.57 with band width of 12.7%, 10.11%	no
[13]	360	3.7, 5.8 with band width of 31%, 13%	no
[15]	2734.29	Center from 1.04 to 1.38 reconfigurable	yes
[17]	314	3.30, 4.83, 5.825, 8.65 with band width of 6.7%, 9.1%, 8.4%, 8.2%	yes
This work	249	3.07–3.29, 4.29–4.73, 5.29–5.71, 8.07–8.78	yes

From Fig. 10(c), when the No. 1 diodes are in the on-state and No. 2 diodes in the off-state, SIR1 has a resonance near 5.6 GHz, and this resonance band overlaps with the first passband of SIR2, which will inevitably have an effect on the first passband of SIR2. As a result, the bandwidth of the third passband of this quad-band BPF becomes narrower when all diodes are in the on state. Table 3 compares the proposed work with other filters.

6. CONCLUSIONS

A novel quad-band passbands filter based on the design of dual E-shaped SIRs is introduced. It consists of a large and a small deformed W-shaped SIR SIRs with a common input and output feed line, and two cross-coupling structures connected to the feed line. The simulated results show that the first passband is 3.07–3.29 GHz; the second pass band is 4.29–4.73 GHz; the third pass band is 5.29–5.71 GHz; and the fourth pass band is 8.07–8.78 GHz. Compared with the basic SIR structure and E-shaped one, the effective area of the miniaturized design is reduced by 62% and 21%, respectively. The diode is introduced as a switch to control the working state of each SIR to achieve the reconfiguration function of the passbands of the quad-band BPF. Due to its reconfigurability, the design can be used for 5G applications.

ACKNOWLEDGMENT

This work was supported by the Key Research and Development Project of Guangdong Province (2020B0101080001).

REFERENCES

1. Al-Yasir, Y., Y. Tu, M. S. Bakr, N. O. Parchin, A. S. Asharaa, W. A. Mshwat, et al., "Design of multi-standard single/tri/quint-wideband asymmetric stepped-impedance resonator filters with adjustable TZs," *IET Microw. Antennas Propag.*, Vol. 13, No. 10, 1637–1645, Aug. 2019.
2. Qiao, Z., X. Pan, F. Zhang, and J. Xu, "A tunable dual-band metamaterial filter based on the coupling between two crossed SRRs," *IEEE Photonics Journal*, Vol. 13, 99, 2021.
3. Li, Z., L. Wang, M. He, X. Li, and Z. Wang, "Compact dual-/tri-/quad-band bandpass filters with independently frequency-tunable and switchable passbands," *International Journal of Microwave and Wireless Technologies*, Vol. 13, No. 4, 322–334, 2020.
4. Tang, W. S., B. J. Xiang, S. Y. Zheng, and Y. L. Long, "Design of wideband/dual-band bandpass filter using a vias and slots loaded sector circular patch resonator," *International Journal of RF and Microwave Computer-Aided Engineering*, Vol. 31, No. 7, Jul. 2021.
5. Xu, W., K. X. Ma, and C. Y. Du, "Design and loss reduction of multiple-zeros dual-band bandpass filter using SISL," *IEEE Transactions on Circuits and Systems*, Vol. 68, 1168–1172, Oct. 2021.
6. Zhu, Y. X., J. Zhang, J. Cheng, H. P. Zhu, J. Hu, and X. Tian, "Compact dual-band bandpass filter with flexible passband frequencies and sharp skirt using cross coupling and mixed magnetic and electric coupling," *International Journal of RF and Microwave Computer-Aided Engineering*, Vol. 31, No. 6, Apr. 2021.
7. Wang, J. P., L. Wang, Y. X. Guo, Y. X. Wang, and D. G. Fang, "Miniaturized dual-mode bandpass filter with controllable harmonic response for dual-band applications," *Journal of Electromagnetic Waves and Applications*, Vol. 23, 1525–1533, Apr. 2012.
8. Maleki, S. J. and M. Dousti, "A compact dual-band bandpass filter using microstrip meander loop and square loop resonators," *IEICE Electron. Express*, Vol. 9, 1342–1348, Aug. 2012.
9. Dai, X. W., C. H. Liang, and Z. X. Chen, "Novel dual-mode dual-band bandpass filter using nested microstrip meander-loop resonators," *Microwave and Optical Technology Letters*, Vol. 50, 836–838, Mar. 2008.

10. Quddious, A., M. Abbasi, A. Saghir, S. Arain, M. A. Antoniades, A. Polycarpou, et al., "Dynamically reconfigurable SIR filter using rectenna and active booster," *IEEE Transactions on Microwave Theory and Techniques*, Vol. 67, No. 4, 1504–1515, Jan. 2019.
11. Gómez-García, R., L. Yang, J.-M. Muñoz-Ferreras, and D. Psychogiou, "Selectivity-enhancement technique for stepped-impedance-resonator dual-passband filters," *IEEE Microwave and Wireless Components Letters*, Vol. 29, No. 7, 453–455, Jun. 2019.
12. Faisal, M., S. Khalid, M. U. Rehman, and M. A. Rehman, "Synthesis and design of highly selective multi-mode dual-band bandstop filter," *IEEE Access*, Vol. 9, 43316–43323, Mar. 2021.
13. Wu, Y.-L., C. Liao, and X.-Z. Xiong, "A dual-wideband bandpass filter based on E-shaped microstrip SIR with improved upper-stopband performance," *Progress In Electromagnetics Research*, Vol. 108, 141–153, 2010.
14. Zhang, R., C.-H. Shao, and D. Peroulis, "A new adaptive reconfigurable bandpass filter with flexible resonance control," *Proceeding of European Microwave Conference*, 539–542, Madrid, Spain, Sept. 2018.
15. Fan, M., K. Song, L. Yang, and R. Gómez-Garcia, "Frequency-reconfigurable input-reflectionless bandpass filter and filtering power divider with constant absolute bandwidth," *IEEE Transactions on Circuits and Systems*, Vol. 68, No. 7, 2424–2428, Jan. 2021.
16. Song, K., M. Fan, and Y. Fan, "Novel reconfigurable bandpass filter with wide tunable bandwidth," *Proceeding of IEEE MTT-S International Wireless Symposium*, 1–3, Guangzhou, China, Aug. 2019.
17. Wang, R., T. Tang, S. Z. Jing, and Y. Fan, "Switch controlled 4 bands band pass filter with two E-shaped SIRs," *Proceeding of IEEE MTT-S International Microwave Workshop Series Advanced Materials Processes RF THz Applications*, 10–12, Chongqing, China, 2021.